Research Article

Baosheng Wu, Jinglin Liu, Qi Song*, Zan Lv, and Wei Bai

Controllability of joint integrity and mechanical properties of friction stir welded 6061-T6 aluminum and AZ31B magnesium alloys based on stationary shoulder

https://doi.org/10.1515/htmp-2019-0001
Received Sep 28, 2018; accepted Nov 08, 2018

Abstract: In order to improve joint integrity and reduce the amount of intermetallic compounds (IMCs), 6061-T6 Al and AZ31B Mg alloys were successfully joined by stationary shoulder friction stir welding (SSFSW). The stationary shoulder effectively enhanced the joint surface integrity and reduced the thickness reduction of the Al/Mg joint. The elimination of pin adhesion was beneficial to increasing material transfer and then improving interfacial joining length of Al/Mg joint. Extremely thin IMCs layer could be achieved because of the heat sink induced by the stationary shoulder. The maximum tensile strength of the Al/Mg joint reached 137 MPa at a welding speed of 60 mm/min, rotating velocity of 1000 rpm and offset to Mg sheet of 0.3 mm, which was 130% higher than that of conventional joint. SSFSW is feasible and has the potential to join dissimilar materials with the formation of IMCs, such as Al/Mg alloys, Al/copper alloys, Al/titanium alloys and so on.

Keywords: Friction stir welding; Stationary shoulder; Aluminum/magnesium alloys; Material flow; Intermetallic compounds; Mechanical properties

1 Introduction

Aluminum (Al) and Al alloys have the advantages of the high strength, good formability, excellent corrosion resistance and weight savings, thereby widely applying in aerospace, automotive, electronics, shipbuilding and so on [1–6]. As the one of lightest structural metals, Magnesium (Mg) alloys have been applied in transportation and electronic industries because of the high specific strength, rigidity and good damping capacities [7–9]. The welding technologies of Al and Mg alloys have been brought into focus in order to utilize the excellent performances of the both materials and optimize structural configuration. It is difficult to join dissimilar materials of Al and Mg alloys by conventional fusion welding techniques because of the coarse grains, hot cracks, pores, especially amounts of hard and brittle intermetallic compounds (IMCs) [10].

As a solid state welding technique, friction stir welding (FSW) can effectively avoid the welding defects associated with conventional fusion welding because of the higher joint quality, smaller distortion, lower residual stress and pollution-free and so on, which has potential to join dissimilar Al/Mg alloys [11–13]. Currently, FSW has successfully achieved high-quality joints of similar Al alloys. However, conventional FSW is difficult to obtain dissimilar Al/Mg joints with acceptable joint integrity, such as surface finishing, thickness reduction, mechanical properties and so on [14, 15]. Yan *et al.* [14] proved that the adhesion materials featured by the IMCs of Al_3Mg_2 and $Al_{12}Mg_{17}$ on the surface of the rotating pin easily resulted in bad joint formation. Yan *et al.* [15] expounded that welding temperature reached eutectic temperature under a rotating velocity of 1000 rpm and welding speed of 30 mm/min, thereby resulting in the crack defects on the joint surface. Furthermore, Sato *et al.* [16] welded 6 mm thick sheets of 1050 Al and AZ31 Mg alloys under 90 mm/min and 2450 rpm and found that the cracks appeared in the stir zone (SZ) when the peak temperature was higher than 460 °C. Mofid *et al.* [17, 18], Zhao *et al.* [19], Wu *et al.* [20] and Ji *et al.* [11, 12, 21] used underwater FSW, stationary shoulder FSW (SSFSW) and ultrasonic assisted SSFSW to join Al/Mg dissimilar materials, respectively. Zhao *et al.*

***Corresponding Author: Qi Song:** School of Aerospace Engineering, Shenyang Aerospace University, Shenyang 110136, People's Republic of China; Email: sauqsong@163.com
Baosheng Wu, Jinglin Liu, Zan Lv, Wei Bai: School of Aerospace Engineering, Shenyang Aerospace University, Shenyang 110136, People's Republic of China
Baosheng Wu and Jinglin Liu contributed equally to this work

[19] performed underwater FSW of Al and Mg alloys and found that the layer of IMCs was thinner than that in air. Mofid *et al.* [17, 18] studied effects of water, air and nitrogen on dissimilar FSW joint of Al and Mg alloys and found that large number of IMCs appeared in SZ under air, while water and nitrogen cooling were propitious to decreasing the number of IMCs. In our pre-experiment, SSFSW was beneficial to improving cooling rate, thereby reducing the amounts of IMCs [22]. Wu *et al.* [20] pointed out that ultrasonic could exert a little preheating effect on the welded workpieces, and did not influence the peak temperature. Meanwhile, Ji *et al.* [11, 12, 21] reported that ultrasonic could break the IMCs into small particles and then address these problems according to the acoustic streaming of ultrasonic based on the stationary shoulder tool.

Optimization of welding parameters in SSFSW of Al/Mg alloys is the key to dominate the joint integrity and mechanical properties. In this study, the effect of welding speed on SSFSW joint was mainly investigated in detail from the aspects of joint integrity, material flow, microstructure and mechanical properties.

2 Experimental procedure

The base materials (BMs) used in this experiment were 3 mm thick 6061-T6 Al and AZ31B Mg alloys sheets. Welding tool system included a stationary shoulder and a rotating tool. The inside and outside diameters of the stationary shoulder tool were 11 mm and 16 mm, correspondingly. The diameters of the shoulder, pin bottom and top of the rotating tool featured by right tapered-and-threaded were 10, 5 and 3 mm, correspondingly. The length of the rotating pin was 2.8 mm. A tilt angle relative to Z-axis was 2.5°. A rotating velocity of 1000 rpm was constant. Welding speeds varied from 30 mm/min to 80 mm/min and the interval was 10 mm/min. The welding tool offset 0.3 mm to advancing side (AS). The welding direction was parallel to the rolling direction of sheets. Figure 1 exhibits the schematic during SSFSW of Al/Mg alloys.

The specimens were cut perpendicular to the welding direction using an electrical discharge machine to conduct the microstructural and mechanical characterizations. The microstructural specimens were respectively etched by the two reagents (2 ml HF, 3 ml HCl, 5 ml HNO_3 and 190 ml H_2O for the Al alloy; 5 ml CH_3COOH + 5 g $C_6H_2OH(NO_2)_3$ + 10 ml H_2O + 100 ml C_2H_5OH for the Mg alloy) and then observed using an optical microscope. Partial smashed particle was presented by a scanning electron microscopy (SEM) with an energy dispersive spectrometer. Microhardness of a typical Al/Mg joint was measured using a micro-hardness tester at a load of 200 g and a dwelling time of 10 s along the thickness direction. The interval between the both adjacent points was 0.5 mm. Three tensile specimens were prepared with reference to ISO 9018 [23]. Tensile tests were carried out at a crosshead speed of 2 mm/min. The fracture surfaces of the tensile specimen were also observed by SEM.

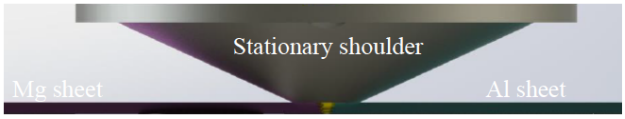

Figure 1: Schematic during SSFSW of Al/Mg alloys

3 Results and discussion

3.1 Material transfer

Figure 2 exhibits the pin adhesion morphologies of the rotating tools at typical welding speeds. The severe pin adhesion was formed at a high heat input induced by a low welding speed of 30 mm/min, thereby making a tapered-and-threaded pin into a tapered pin without thread. The material transfer induced by the tapered pin was worse than that of the tapered-and-threaded pin [24]. The frictional heat decreased and the adhesion phenomenon was eliminated with increasing welding speed to 60 mm/min, as displayed in Figure 2b. The shape of the tapered-and-threaded pin remained unchanged under the welding speeds of 60 mm/min and 80 mm/min. The ability of the tapered-and-threaded pin to drive the plasticized materials was enhanced compared with the tapered pin without thread because of the elimination of the adhesion phenomenon. Meanwhile, the volume of the driven materials increased and the material transfers through the vertical and horizontal directions were improved, thereby transforming much more materials from the bottom to the top of the rotating pin. Meanwhile, the material transfer models under conventional FSW and SSFSW processes are displayed in Figure 3. Moreover, the stationary shoulder effectively prevents the plasticized materials overflowing out of the SZ and then reduces the size of flashes, while much more materials can flow into the SZ [25, 26]. The instantaneous cavity can be filled with the abundant plasticized materials. The welding defects, such as flashes and cavities, are prone to be reduced or even eliminated under the synergistic effects.

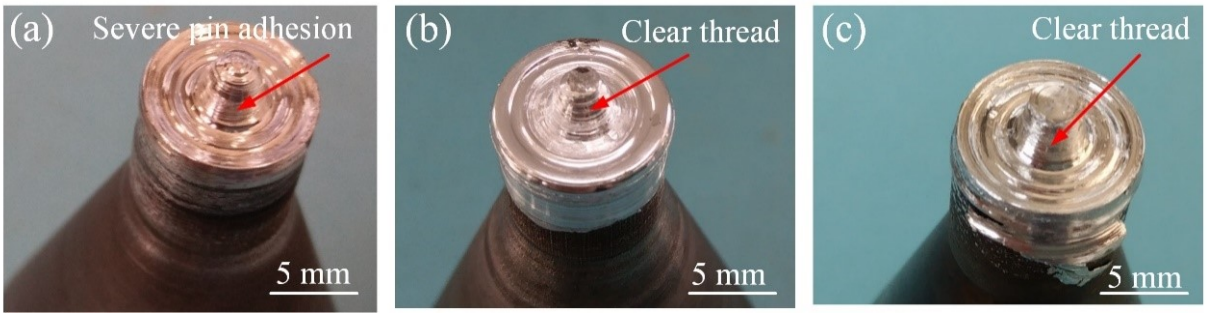

Figure 2: Morphologies of rotational tool after welding based on stationary shoulder process at typical welding speeds: (a) 30 mm/min, (b) 60 mm/min and (c) 80 mm/min

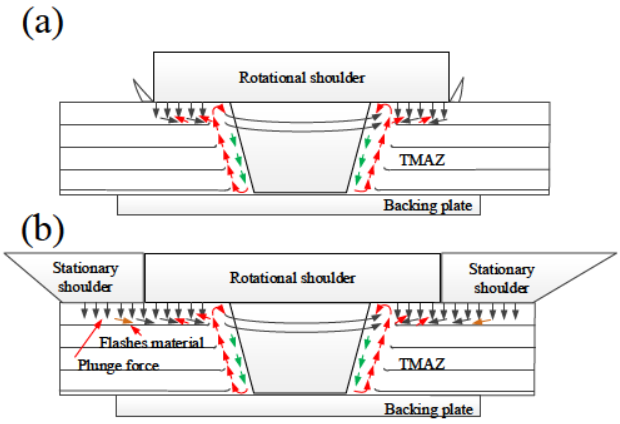

Figure 3: Material flow behaviors using different welding processes: (a) conventional FSW and (b) SSFSW

3.2 Surface integrity

Figure 4 displays the surface integrity of the SSFSW joints under different welding speeds. The high frictional heat leaded to the severe rotating tool adhesion when welding speed was 30 mm/min or 40 mm/min. This phenomenon caused the surface of the rotating shoulder to be higher than that of the stationary shoulder, thereby leading to the deep shoulder marks (Figures 4a and 4b). As the welding speed increased to 50 mm/min, 60 mm/min and 70 mm/min, the size of the shoulder marks drastically reduced, as displayed in Figures 4c-4e. One of the most important reasons is that increasing welding speed leads to the reductions in the heat input and the pin adhesion. This problem of pin adhesion can be solved by reducing heat input under a high welding speed, thereby improving the vertical material flow and reducing the outflowing of material from the SZ. The good surface integrity of the joint could be obtained by regulating and controlling welding speed. In the meantime, the elimination of the flash defects resulted in the micro thickness reduction, which was propitious to improving the ability of load bearing. The frictional heat further reduced with further increasing the welding speed to 80 mm/min, thereby resulting in the more discontinuous groove defect on the joint surface (Figure 4f).

3.3 Macrostructure

The macrostructures of the joints under different welding speeds are displayed in Figure 5. The welding speed had an important influence on the macrostructures in cross-section. The severe adhesion phenomenon occurred on the surface of the rotating tool at a welding speed of 30 mm/min. This phenomenon was difficult to increase the vertical transfer of the plasticized materials, thereby leading to a cavity defect with large size, as exhibited in Figure 5a. With increasing welding speeds to 40 mm/min and 50 mm/min, the size of the cavity defects gradually reduced due to the reduction of the pin adhesion. As the welding speed further reached 60 mm/min, the sound joint was attained (Figure 5d). This is because that the clear thread in Figure 2b is observed on the surface of the rotating tool because of the elimination of the pin adhesion. However, when the welding speed was 70 mm/min, the cavity defect appeared again because of the insufficient material flow induced by the low frictional heat under the condition without the pin adhesion, as indicated in Figure 5e. For FSW of Al/Mg alloys, the low welding speed leads to the longer time of stir action and the higher heat input, thereby resulting in the pin adhesion phenomenon and deteriorating the joint formation. Although increasing welding speed is beneficial to reducing the pin adhesion and excessively increasing welding speed may cause the insufficient material transfer, forming the cavity defects. Therefore, the welding speed of 60 mm/min was optimum for the improvement of the joint integrity for the 3 mm thick 6061-T6 and AZ31B alloys sheets.

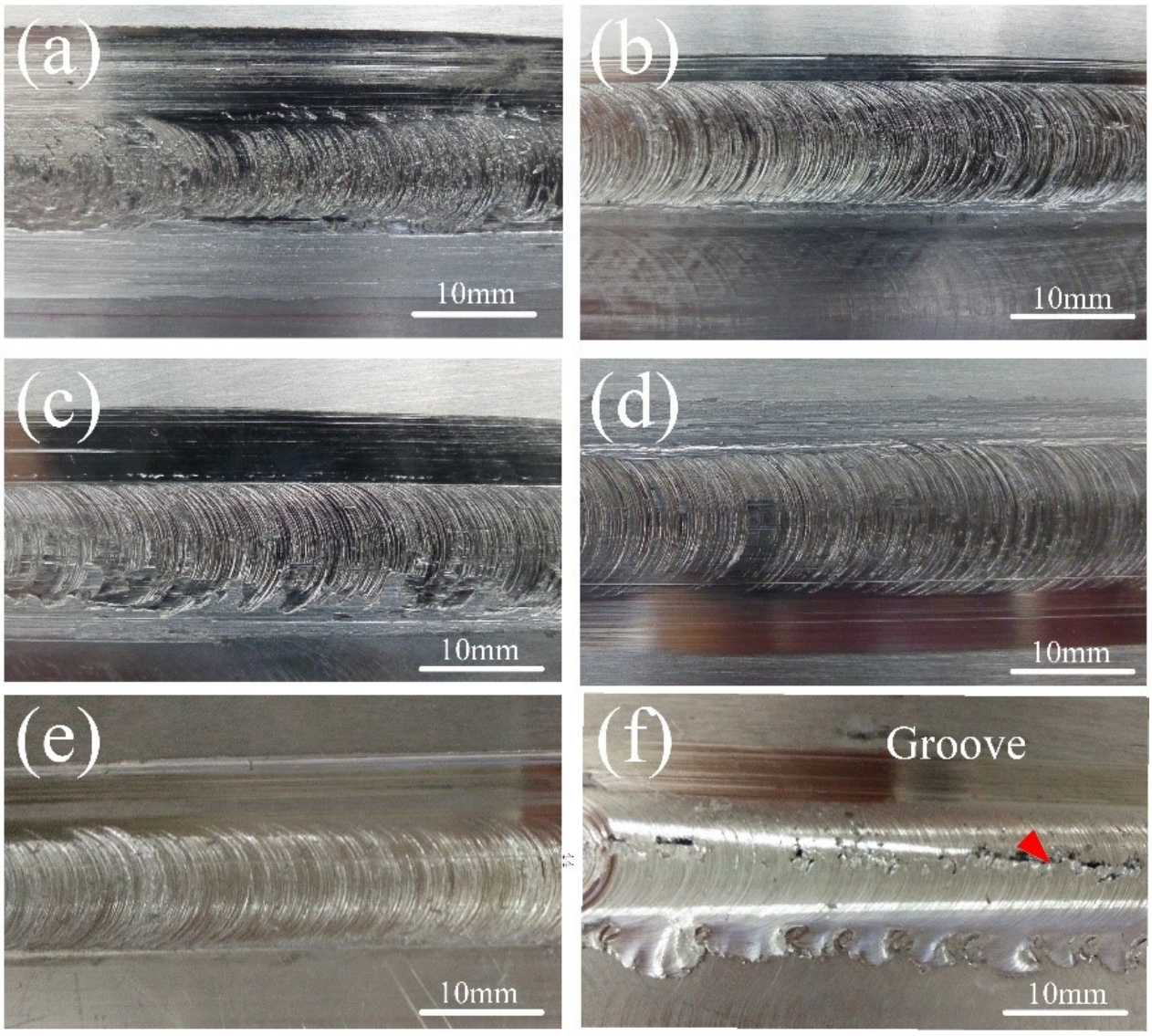

Figure 4: Surface integrity of the SSFSW joints at different welding speeds: (a) 30 mm/min, (b) 40 mm/min, (c) 50 mm/min, (d) 60 mm/min, (e) 70 mm/min and (f) 80 mm/min

3.4 Microstructure

The typical Al/Mg joint was divided into four regions: BM, heat affected zone (HAZ), thermo-mechanically affected zone (TMAZ) and SZ, as displayed in Figure 5d. Figure 6 exhibits the microstructures at different positions marked in Figure 5d. The strength is dominated by the microstructures of the SZ for the Al/Mg joint, especially the Al/Mg joining interface. There was no crack at the interface of Al/Mg joint at different positions, while the interlayer in SZ was complex. The mechanical interlocking was beneficial to improving the tensile properties. Importantly, the white bands appeared at the Al/Mg joining interfaces at the both AS and retracting side (RS) (Figures 6g and 6h). The white bands were corresponding to elements of the IMCs, which had been reported by Zhao *et al.* [19]. Moreover, the Al/Mg joining interface at the RS was far longer and more complex than that at the AS. Firouzdor *et al.* [27] and Huang *et al.* [28] found that the longer interfacial length and the interpenetrating feature thickness were beneficial to improving mechanical interlocking. Therefore, the strength of the joining interface at the RS may be stronger than that at the AS.

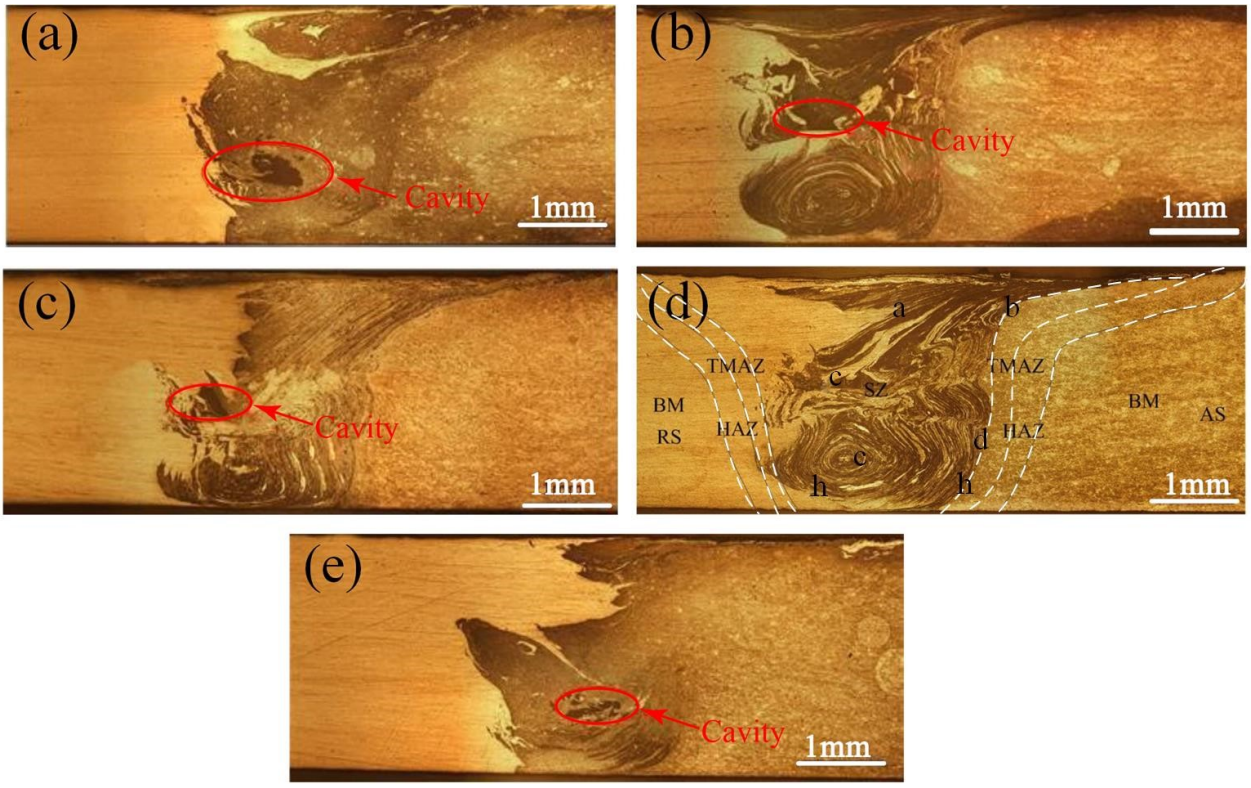

Figure 5: Macrostructures in cross-section of the Al/Mg joints at different welding speeds: (a) 30 mm/min, (b) 40 mm/min, (c) 50 mm/min, (d) 60 mm/min and (e) 70 mm/min

3.5 Mechanical properties

Microhardness distribution of the dissimilar Al/Mg joint is displayed in Figure 7. The hardness of the dissimilar Al/Mg joint exhibited an uneven distribution, which was closely related to strengthening phase distribution and grain size. Especially, size and distribution of the IMCs easily leaded to the non-uniform distribution of hardness [21]. The maximum hardness value in Figure 7 is 128 Hv, which is higher than those of both BMs. The IMCs can improve the microhardness. The hardness variations of other locations in the SZ were dominated by the interlayer microstructures and grain size induced by the degree of dynamic recrystallization.

Figure 8 displays the tensile test results of the Al/Mg joints at different welding speeds. The tensile properties firstly increased and then slightly decreased with the increase of welding speed. The maximum tensile strength and elongation respectively reached 137 MPa and 1.6% under the welding speed of 60 mm/min, which were far higher than those of conventional joint [13]. As mentioned above, the cavity defects induced by the pin adhesion formed in the SZ under the welding speeds lower than 60 mm/min. This defect often leaded the stress concentration and the reduction of loading area, thereby reducing the tensile properties of the Al/Mg joint. The defect-free joint with the longer interface joining layer at the Al/Mg joint interface of the SZ was attained under a welding speed of 60 mm/min, which could bear big load and then enhance the tensile properties. The cavity defects induced by the inadequate material transfer appeared in the SZ again at the welding speeds of 70 mm/min and 80 mm/min, thereby reducing the tensile properties. Liu *et al.* [29] stated that an introduction of ultrasonic into SSFSW of Al/Mg alloys could material flow behavior and eliminate welding defects, which further expanded the welding speed ranges from 60 mm/min to 80 mm/min.

Figure 9 displays the fracture locations of the SSFSW Al/Mg joints at different welding speeds. Obviously, there were two fracture mechanisms, which were the fracture along the welding defects and the fracture along the continuous IMCs layer at the SZ, respectively. When the welding speed varied from 30 mm/min to 50 mm/min, the welding defect appears at the SZ, which leaded to the initiation of the cracks and then further propagates along the Al/Mg joining interface during tensile test (Figures 9a-9c). The continuous IMCs layer occurred at the Al/Mg joining interface of the sound joint at the welding speed of 60 mm/min.

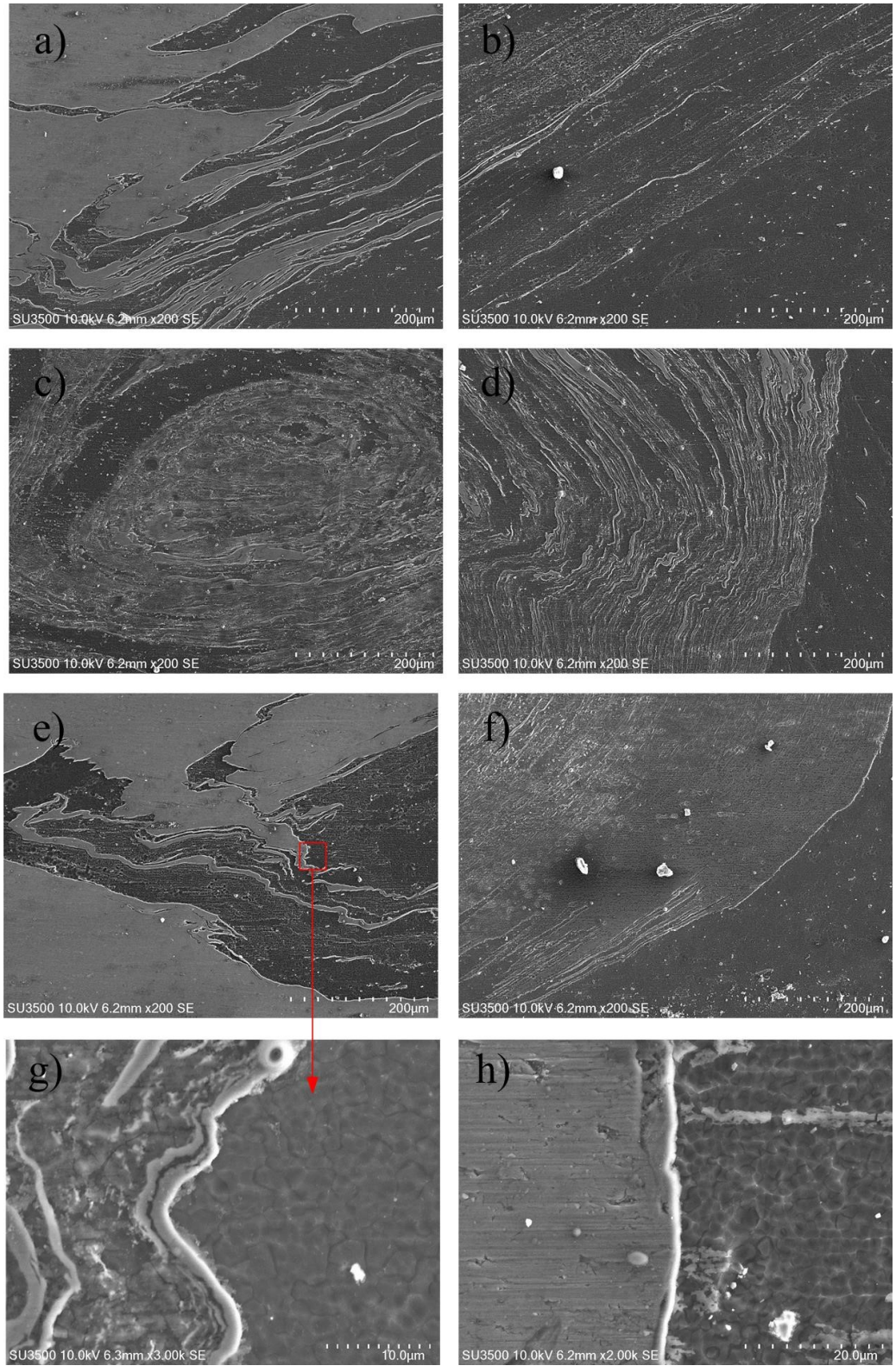

Figure 6: Microstructures at different locations marked in Figure 5d of joint at the welding speed of 60 mm/min and rotational speed of 1000 rpm

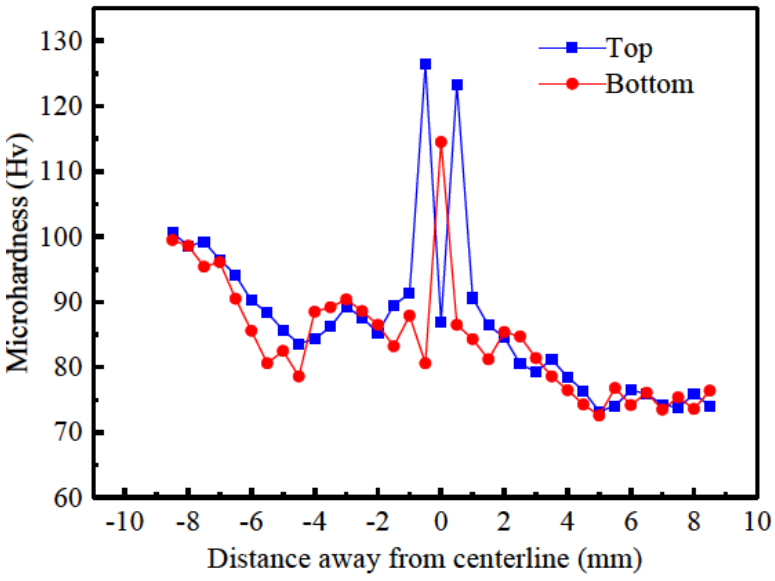

Figure 7: Hardness of the typical Al/Mg joint

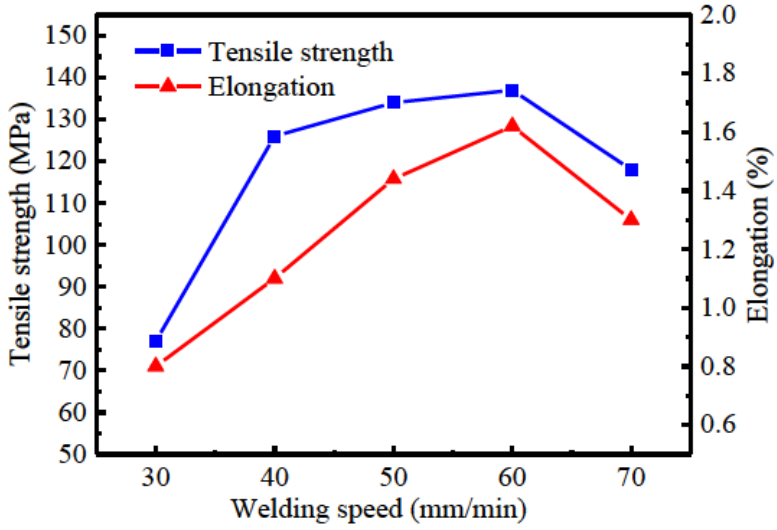

Figure 8: Tensile properties of the Al/Mg joints based on SSFSW

The incompatible deformation appeared at the Al/Mg joining interface because of the hard and brittle IMCs during the bigger tensile load, which easily leaded to the stress concentration and the initiation of the cracks. In this study, the interfacial joining length of the RS was bigger than that of the AS, thereby resulting in the joint fracture at the joining interface between the SZ and the TMAZ of AS (Figure 9d). As the welding speed further increased to 70 mm/min, the fracture location occurred at the cavity defect (Figure 9e). Therefore, the welding defects induced by the adhesion phenomenon and the reduction of heat input were the prominent reason of the joint fracture, while the IMCs layer was the main factor for the sound joint.

Fracture surface morphologies of the typical Al/Mg joint at the welding speed of 60 mm/min were shown in Figure 10. All the fracture surface morphologies through the thickness direction were featured by the cleavage feature (Figures 10b-10d), illustrating the typical brittle fracture because of the occurrence of the IMCs. The fracture morphologies in Figure 10 were consistent with the fracture location of the Al/Mg joint in Figure 10d.

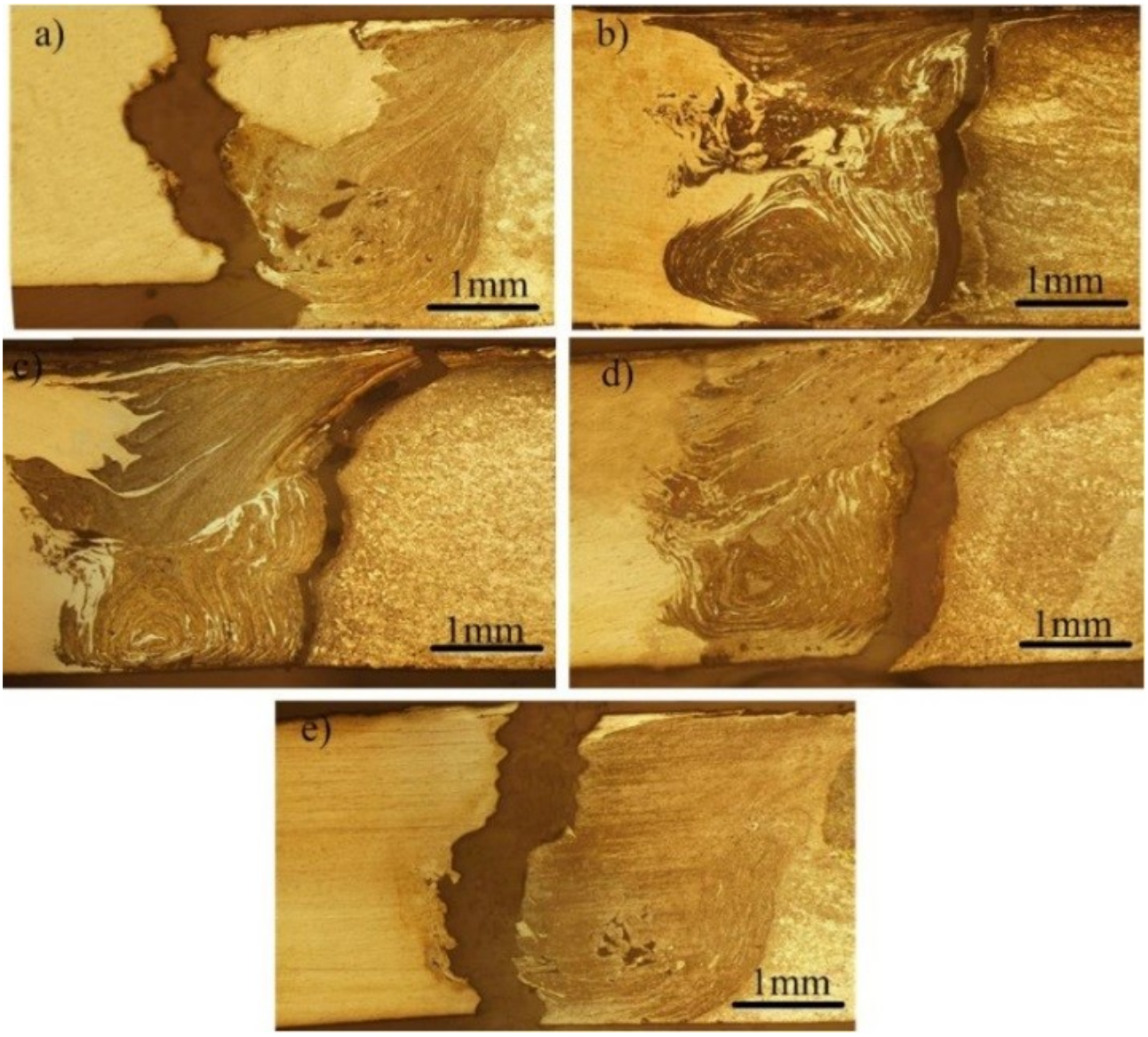

Figure 9: Fracture locations of the joints by different welding speeds: (a) 30 mm/min, (b) 40 mm/min, (c) 50 mm/min, (d) 60 mm/min and (e) 70 mm/min

4 Conclusions

In order to improve joint integrity and reduce thickness reduction and IMCs, 6061-T6 Al and AZ31B Mg alloys were joined by SSFSW. Meanwhile, surface integrity, material transfer, microstructure and mechanical properties of the Al/Mg joint were mainly investigated. Based on the present investigations, the following conclusions can be drawn:

(1) Defect-free joint with good surface integrity and micro thickness reduction could be obtained based on SSFSW under the optimum welding parameter.

(2) The stationary shoulder tool could eliminate the pin adhesion and then enhance material transfer, which was propitious to increasing the mixture degree of the Al/Mg alloys and then improving mechanical interlocking and interface joining length. Meanwhile, the extremely thin IMCs layer formed at the Al/Mg joining interface because of the fast cooling rate induced by the stationary shoulder.

(3) The tensile properties firstly increased and then decreased with the increase of welding speed. The maximum tensile strength of 137 MPa was achieved under the welding speed of 60 mm/min, which was far higher than that of conventional joint.

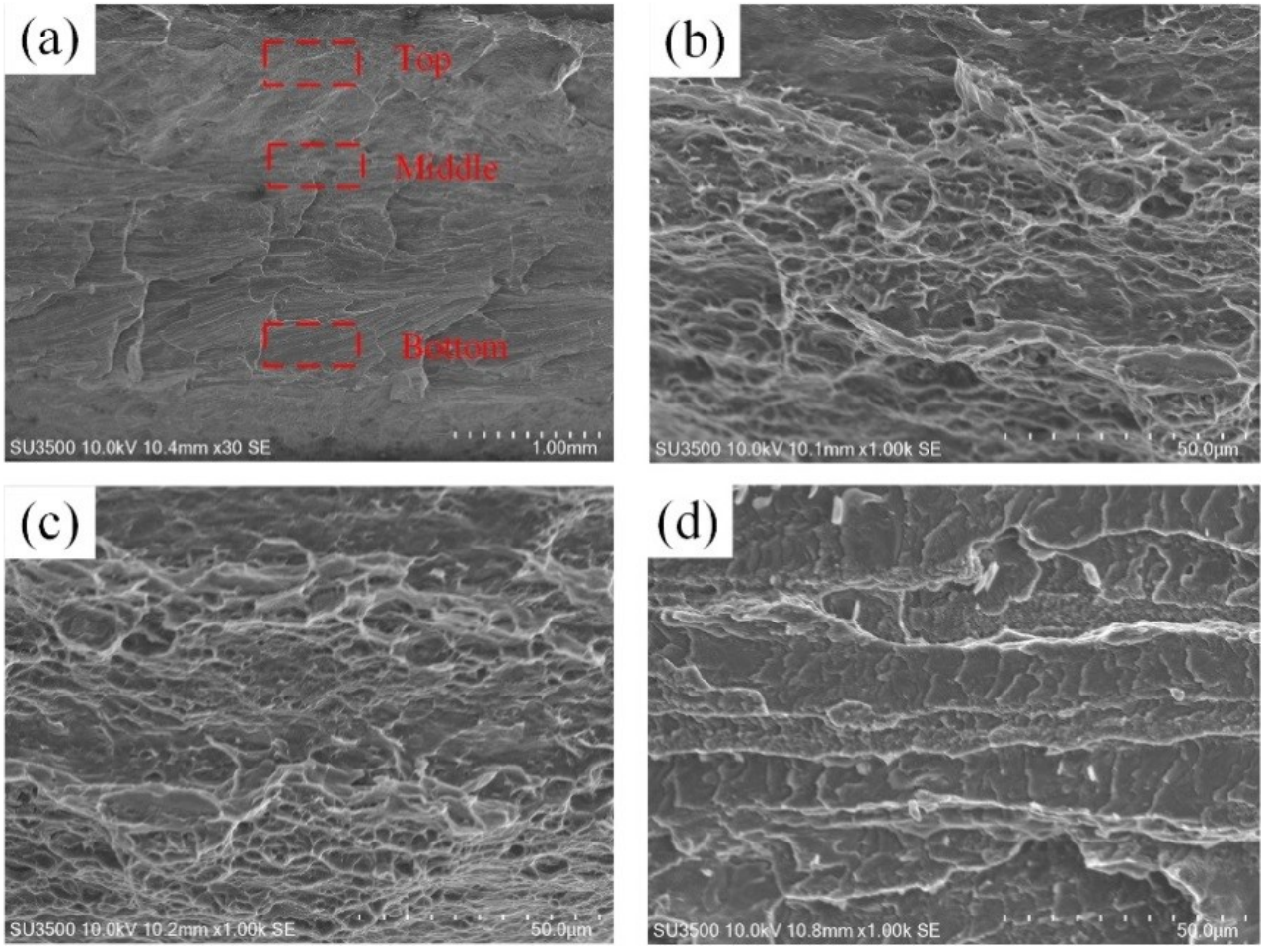

Figure 10: Fracture surface morphologies at the welding speed of 60 mm/min: (a) macroscopic of fracture surface; micro fracture surfaces at different locations in Figure 10a: (b) position b, (c) position c and (d) position d

(4) The SSFSW has potential to join dissimilar materials, such as Al/Mg alloys, Al/copper alloys, Al/titanium alloys and so on, from the viewpoints of good surface integrity, no pin adhesion, micro thickness reduction and extremely thin IMCs layer.

Acknowledgement: This work is supported by the National Natural Science Foundation of China (No. 51705339) and the Education Department Foundation of Liaoning Province (L201615).

References

[1] L. Wan, Y. Huang, W. Guo, S. Lv, J. Feng, J. Mater. Sci. Technol. 30 (2014) 1243–1250.
[2] Y.X. Huang, L. Wan, S.X. Lv, Z. Zhang, H.J. Liu, Sci. Technol. Weld. Join. 17 (2012) 636–642.
[3] Z. Liang, X. Wang, C. Cai, D. Wang, High Temp. Mater. Proc. (2018).
[4] Y. Chen, H. Liu, J. Feng, Mater. Sci. Eng. A 420 (2006) 21–25.
[5] H.J. Liu, H. Fujii, M. Maeda, K. Nogi, J. Mater. Process. Technol. 142 (2003) 692–696.
[6] S.D. Ji, X.C. Meng, R.F. Huang, L. Ma, S.S. Gao, Mater. Sci. Eng. A 664 (2016).
[7] Q. Wen, Y. Yue, S. Ji, Z. Li, S. Gao, High Temp. Mater. Process. 35 (2016) 375–379.
[8] X. Cao, M. Jahazi, Mater. Des. 30 (2009) 2033–2042.
[9] W.Y. Li, T. Fu, L. Hütsch, J. Hilgert, F.F. Wang, J.F. dos Santos, N. Huber, Mater. Des. 64 (2014) 714–720.
[10] H. Shi, K. Chen, Z. Liang, F. Dong, T. Yu, X. Dong, L. Zhang, A. Shan, J. Mater. Sci. Technol. 33 (2017) 359–366.
[11] X. Meng, Y. Jin, S. Ji, D. Yan, J. Mater. Sci. Technol. 34 (2018) 1817–1822.
[12] S. Ji, X. Meng, Z. Liu, R. Huang, Z. Li, Mater. Lett. 201 (2017) 173–176.
[13] Z. Liu, S. Ji, X. Meng, J. Mater. Eng. Perform. 27 (2018) 1404–1413.
[14] T. Nakkeran, S. Muthukumran, P.A. Dhanush, Trans. Nonferrous Met. Soc. China 20 (2010) s619–s623.
[15] J. Yan, Z. Xu, Z. Li, L. Li, S. Yang, Scr. Mater. 53 (2005) 585–589.

[16] Y.S. Sato, S.H.C. Park, M. Michiuchi, H. Kokawa, Scr. Mater. 50 (2004) 1233–1236.
[17] M.A. Mofid, A. Abdollah-zadeh, F. Malek Ghaini, Mater. Des. 36 (2012) 161–167.
[18] M.A. Mofid, A. Abdollah-Zadeh, F.M. Ghaini, C.H. Gür, Metall. Mater. Trans. A Phys. Metall. Mater. Sci. 43 (2012) 5106–5114.
[19] Y. Zhao, S. Jiang, S. Yang, Z. Lu, K. Yan, Int. J. Adv. Manuf. Technol. 83 (2016) 673–679.
[20] X. LÜ, J. Mech. Eng. 52 (2016) 58.
[21] Z. Liu, X. Meng, S. Ji, Z. Li, L. Wang, J. Manuf. Process. 31 (2018) 552–559.
[22] S. Ji, R. Huang, X. Meng, L. Zhang, Y. Huang, J. Mater. Eng. Perform. 26 (2017) 2359–2367.
[23] G. 2650–2008/ISO 9016: 2001., (2008).
[24] Y. Huang, Y. Xie, X. Meng, Z. Lv, J. Cao, J. Mater. Process. Technol. 252 (2018) 233–241.
[25] J.Q. Li, H.J. Liu, Int. J. Adv. Manuf. Technol. 66 (2013) 623–634.
[26] Y. Huang, X. Meng, Y. Xie, J. Li, L. Wan, Compos. Part A Appl. Sci. Manuf. 112 (2018).
[27] V. Firouzdor, S. Kou, Metall. Mater. Trans. A Phys. Metall. Mater. Sci. 41 (2010) 2914–2935.
[28] Y. Huang, X. Meng, Y. Xie, L. Wan, Z. Lv, J. Cao, J. Feng, Compos. Part A Appl. Sci. Manuf. 105 (2018) 235–257.
[29] Z. Liu, S. Ji, X. Meng, Int. J. Adv. Manuf. Technol. 97 (2018) 4127–4136.